Controlled extrinsic magnetoelectric coupling in BaTiO3/Ni nanocomposites: Effect of compaction pressure on interfacial anisotropy

C. Brosseau, Vincent Castel, Michel Potel

Controlled extrinsic magnetoelectric coupling in $BaTiO_3$/Ni nanocomposites: Effect of compaction pressure on interfacial anisotropy

C. Brosseau,[1,a] V. Castel,[1] and M. Potel[2]
[1]*Lab-STICC, Université Européenne de Bretagne, Université de Brest, CS 93837, 6 avenue Le Gorgeu, 29238 Brest Cedex 3, France*
[2]*Unité Sciences Chimiques de Rennes, Equipe Chimie du Solide et Matériaux, Université de Rennes 1, 35042 Rennes Cedex, France*

(Received 6 May 2010; accepted 17 June 2010; published online 22 July 2010)

The dynamical control of the dielectric response in magnetoelectric (ME) nanocomposites (NCs) renders an entire additional degree of freedom to the functionality of miniaturized magnetoelectronics and spintronics devices. In composite materials, the ME effect is realized by using the concept of product properties. Through the investigation of the microwave properties of a series of $BaTiO_3$/Ni NCs fabricated by compaction of nanopowders, we present experimental evidence that the compaction (uniaxial) pressure in the range 33–230 MPa affects significantly the ME features. The Ni loading was varied from zero ($BaTiO_3$ only) to 63 vol %. Our findings revealed that the ME coupling coefficient exhibits a large enhancement for specific values of the Ni volume fraction and compaction pressure. The coupling effects in the NCs were studied by looking at the relationships among the crystallite orientation and the magnetic properties. The magnetization curves for different directions of the applied magnetic field cannot be superimposed. We suggest that the average magnetization measurements on these NCs under compressive stress are dominated by strain anisotropy rather than magnetocrystalline anisotropy. Overall, these observations are considered to be evidence of stress-induced microstructural changes under pressure which strongly affect the elastic interaction between the magnetostrictive and piezoelectric phases in these NCs. These results have a potential technological impact for designing precise tunable ME NCs for microwave devices such as tunable phase shifters, resonators, and delay lines. © *2010 American Institute of Physics*. [doi:10.1063/1.3465549]

I. INTRODUCTION

An intensifying experimental effort is under way aimed at understanding and utilizing magnetoelectric (ME) nanocomposites (NCs). This is due to the new physics that can be studied, such as product properties and dynamical coupling between electric and magnetic-dipole moments,[1] and microwave damping.[2–6] The initial impetus driving ME materials was the prospect of employing a single temporally varying electric field excitation, e.g., voltage gradient, to tune both polarization and magnetization characteristics. These multifunctional materials at and above room temperature present enormous potential for attendant device applications,[7] e.g., frequency-agile miniaturized antennas, electric field-controlled microwave resonance devices, microelectromechanical and nanoelectromechanical systems, spintronics, and data-storage media.[8,9] However, despite large research effort, these materials have a number of striking fundamental properties which are not fully understood. The challenge, as far as theoretical studies are concerned, is the relative complexity of these systems and of the theories needed to describe the coupling between polarization and magnetization mechanisms, i.e., the mechanism driving the magnetoelectricity in such systems.[1,10,11] From the experimental standpoint, frequency-domain spectroscopy and broadband ferromagnetic magnetic resonance have proved to be useful tools in characterizing the gigahertz frequency electromagnetic response of ME NCs and the dynamical aspect of the ME coupling.[2–6,12–15] Possible implementation of device applications relies upon a significantly improved understanding and ability to dynamically control this response. Although most of the contemporary activity has been focused in understanding the ME properties of laminate inhomogeneous materials,[1,16–19] recently the interest has shifted toward granular two-phase nanostructures where the electric polarization and the magnetic moment are intrinsic to the two different phases, but coupled by interfacial strain.[2–6,20–23] Although laminated ME composites exhibit larger ME response, powder technology provides advantages such as cost effectiveness, easy fabrication process, better control of the process parameters, and fabrication of large volumes. Recently we have reported that an optimum magnetic field bias H of ≈ 100 kOe exists which produced a room temperature ME response, $[\varepsilon(H)-\varepsilon(0)]/\varepsilon(0)$, of 300% at resonance, where $\varepsilon(H)$ denotes the effective permittivity of a Ni/$BaTiO_3$ NC containing 17.1 vol % of Ni.[4] The debate over the origin of the ME effect continues today, with some researchers suggesting to probe the magnetoelastic coupling between the magnetostrictive and piezoelectric phases from the measurement of the effective complex permittivity ε and magnetic permeability μ since these quantities are the standard source of information on the response to external electric and magnetic fields.[2–6,12–15,24] No surprise that from the very beginning two key issues have been hotly debated in the

[a]Electronic mail: brosseau@univ-brest.fr.

field: the strength of the coupling between polarization and magnetization mechanisms and the role of interface.

Beyond compositional changes, there has been an ongoing interest in the nature of structural transformations in nanoparticles (of typical size below 100 nm) systems under high pressure. Indeed, pressure offers the opportunity to drastically modify the electronic, magnetic, or thermomechanical properties of NCs. In experiments on multiferroic materials, it has been observed[1,25–28] that the anomalies in the permittivity that occur at the onset or with changes in the magnetic order are generally associated with lattice distorsions. This suggests that the ME coupling proceeds via the lattice atomic displacements. For example, varying the degree of strain can be realized by choosing different orientations of the substrate which yields different phase morphologies in self-assembled epitaxial NC films. Related to this effect, the question of the role of compaction pressure as a mechanism to modify the ME properties via the microstructure has not been addressed in detail. The difficulty in controlling the bulk ME property of granular NCs is rooted in the complexity of the electric and magnetic dipoles properties of interfaces of these strongly correlated materials.[29] In this paper, we expand on our previous work[5] in which a tentative explanation of the relevant mechanism that underlies the ME effect in $Ni/BaTiO_3$ NCs in the microwave range of frequencies was proposed, based on striction across the interfaces between the magnetic and piezoelectric phases. Additional evidence in support of this picture was found in recent spin-wave dynamics experiments.[30] Here, we report complementary observations on $Ni/BaTiO_3$ NCs, when fabrication process modifications are used. While strong electric response is obtained naturally in high-ε materials, i.e., $BaTiO_3$, the challenge from the ME point of view is to obtain a strong magnetic response and for this reason, we will use a metallic component, i.e., Ni. One important task is to understand and control the interplay between magnetic and elastic properties.

In light of these recent developments the major issue that we address in this paper is the impact of compaction pressure on the microwave (ε, μ), magnetostatic, and dc conductivity characteristics of $Ni/BaTiO_3$ NCs which offers the opportunity to investigate the ME coupling in two-phase nanostructures. The literature reports few experimental studies of the physical mechanisms that control this product property in granular NCs at high frequencies. Of particular interest are those activities that involve crystallites of nanosized diameter since they have a large number of atoms within their effective surface area versus their volume.[31] In addition, it has been widely recognized that mechanical stability, hardness, sintering ability, and compressibility are under the dependence of the particle size.[32] Despite the numerous experimental results that have appeared in the literature in the past few months, the importance of the microstructure characterization of the coexisting phases in these complex NCs, and how the compaction pressure can affect this microstructure are still not fully understood. So far, limited data on local structural inhomogeneity at the interface of the nanoclusters which play a pivotal role in the extrinsic ME effect are available. Equally important is addressing the following key questions: does the host matrix (the more dense nanoparticle phase) able to accommodate and relax the strains? How the local environment can be distorted in a magnetic (electric) field by virtue of the spin-orbit coupling? How the compaction pressure leads to mechanical stress redistribution to the Ni and $BaTiO_3$ nanoparticles interface? By the combination of various analytical methods including scanning electron microscopy (SEM), atomic force microscopy (AFM), vibrating sample magnetometry (VSM), and microwave spectroscopy, the present study provides insights into the ME features of granular heterostructures. These issues are certainly among the fundamental aspects of ME NCs that must be addressed before we can come to a complete understanding of the physics of these materials.

Our primary results are as follows. First, we report on an extensive study of the pressure dependence of the crystalline lattice parameters, the saturation magnetization M_s, the coercivity H_c, and the remanent magnetization M_r normalized to M_s (squareness), M_r/M_s. Based on our experiments, we suggest that during the fabrication of these NCs intrinsic stress induces magnetic anisotropy for which strain anisotropy rather magnetocrystalline anisotropy plays a crucial role. Second, from microwave spectroscopy we quantify the magnetic field-induced ε and μ over an extended range of compaction pressure, p, used during production of the NCs. We report significant changes of the complex ME coupling coefficient which is measured by $\alpha_\varepsilon = (\partial\varepsilon/\partial H)_T = \alpha'_\varepsilon - j\alpha''_\varepsilon$. Our results directly address the role of the boundary on α_ε via its dependence versus p. These results illustrate the importance of the delicate balance between short-range striction effects and long-range (dipole) interactions in these interfacial phenomena.

The rest of the paper is structured as follows. Section II outlines a brief description of sample fabrication and measurement procedures. In Sec. III the structural characterization by means of SEM, x-ray diffraction (XRD), and AFM is reported. In Sec. IV we present room temperature magnetization versus field data and microwave response at magnetic fields for all the NCs. The observed compaction pressure dependence of the magnetization properties and ME coupling coefficient is presented and discussed. We discuss the possible mechanisms underlying our observations. The paper closes with a brief summary of our conclusions.

II. SAMPLE PREPARATION AND EXPERIMENTAL DETAILS

The starting powder materials, i.e., spherical $BaTiO_3$ and Ni nanoparticles of average size 35 nm and 30 nm, respectively, were purchased from Nanostructured & Amorphous Materials, Inc. with a nominal purity of 99.9% and used as supplied. High-resolution transmission electron microscopy (TEM) provided both bright-field and high-resolution images (not shown) of the different powders.[5] A series of $Ni/BaTiO_3$ NCs were fabricated at room temperature by mixing prescribed amounts of $BaTiO_3$ and Ni, and pressed into pellet form with p in the range 33–230 MPa. For each loading, a set of toroidal (APC-7-sized) samples was uniaxially pressed with an inner radius of 3 mm, outer radius of 7 mm, and

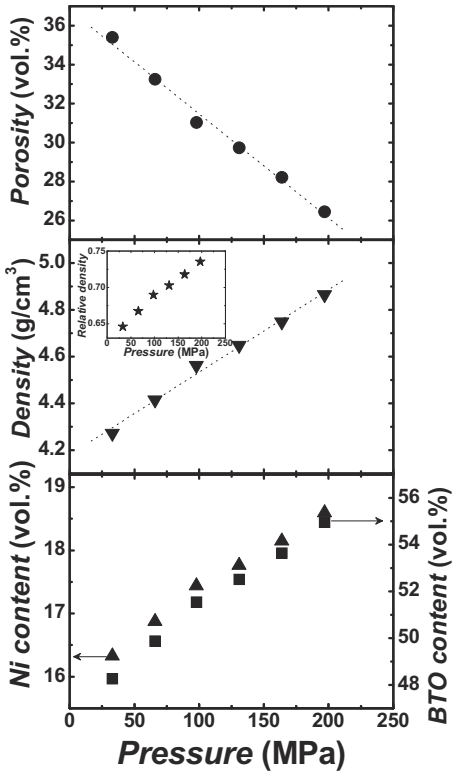

FIG. 1. Upper panel: porosity calculated at different compaction pressures. Room temperature. The dotted line is a guide to the eye. Middle panel: density measured at different compaction pressures. The dotted line is a guide to the eye. The inset shows the relative density, i.e., equal to 1-porosity, vs compaction pressure; lower panel: summary of the nominal compositions in volume percent for all samples in the p range investigated.

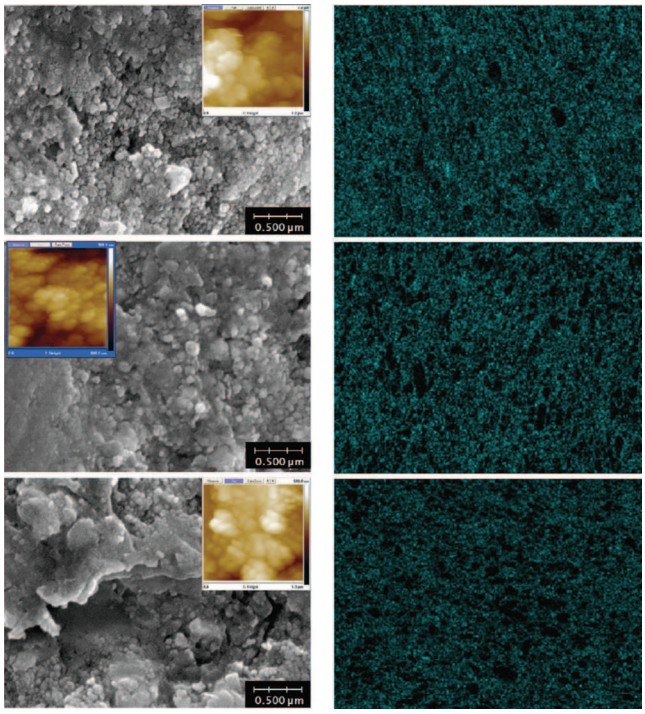

FIG. 2. (Color online) Left panel: SEM micrographs of the $BaTiO_3$/Ni NC sample containing 17.1 vol. % of Ni and selected values of the compaction pressure. From top to bottom: 33 MPa, 98 MPa, and 164 MPa, respectively. The inset shows the corresponding surface-topography AFM images. Right panel: energy dispersive spectrometry images of the corresponding samples, showing the distribution of Ni particles and aggregates bright (blue-green) pixels.

thickness of 3.2 mm. Details of the sample preparation have already been published elsewhere.[4,5] An interesting perspective on these samples is provided in the top panel of Fig. 1, where the porosity is plotted as a function of p. The calculated porosity decreased linearly from 26 vol % (p =230 MPa) to 35 vol % (p=33 MPa). The dashed line through the data indicates a monotonic increase in the density with increasing p. The inset of Fig. 1(b) shows the difference in densification of the powder compacts between 33 and 230 MPa. Figure 1(c) summarizes the nominal compositions in volume percent for all samples in the p range investigated.

SEM (high-resolution SEM, Hitachi S-3200N working at 100 keV) was also used to observe the fractured surface of the samples. Cross-section SEM samples were prepared by cutting the samples into horizontal slices and mechanically polishing them carefully (in two steps). Figure 2 (left) shows representative selected SEM images. Since these images have been obtained in identical experimental conditions, the observed differences reflect the mesostructure differences caused by compaction. To address the possible nonuniformity of the distribution of Ni nanoparticles in the NCs, we have carried out a systematic x-ray microanalysis at the SEM. Figure 2 (right) depicts the map of the chemical composition in a typical sample, i.e., Ni particles and aggregates are represented by bright (blue-green) pixels, as obtained from SEM energy dispersive spectrometry mapping of elements. The microanalysis confirms the magnetic uniformity of the samples.

For present purposes we also examined AFM images. To do so, a Nanoscope V multimode atomic force microscope from Veeco Digital Instruments was used. For AFM observations, a Veeco microetched phosphorous doped silicon tip, with radius=5 nm, was used in the vibrating-lift mode. The tip velocity was in the range 10–20 μm s^{-1}. We examined cross-sections of the samples, prepared by mechanical polishing using fine abrasive papers (down to 1200 grade) and diamond powders with a water-free lubricant. This polishing provides a very flat and smooth surface required for AFM measurements. Examples of surface topographies are shown in the inset of the SEM images of Fig. 2 (left). These images show a strongly heterogeneous microstructure: bright areas are high structures while dark domains correspond to low structures. Such observation is important because grain boundaries are known or suspected to influence functionality of the NCs. In addition, many large and unconnected pores are visible.

XRD measurements of as-grown samples were performed to check for phase purity and to determine the lattice parameters. $\theta/2\theta$ scans with the Bragg–Brentano geometry were collected at room temperature under air ambient using a Bruker D8 Advance equipped with the LynxEye detector for precise determination of the cell parameters. The x-ray source was monochromatic Cu $K_{\alpha 1}$ radiation (1.5406 Å) with accelerating voltage 40 kV and tube current of 40 mA. The XRD spectra were acquired with a scanning step resolution of 0.010 4725° in the 2θ range from 15° to 130° and the step time was 358 s. XRD patterns were analyzed using the FULL-

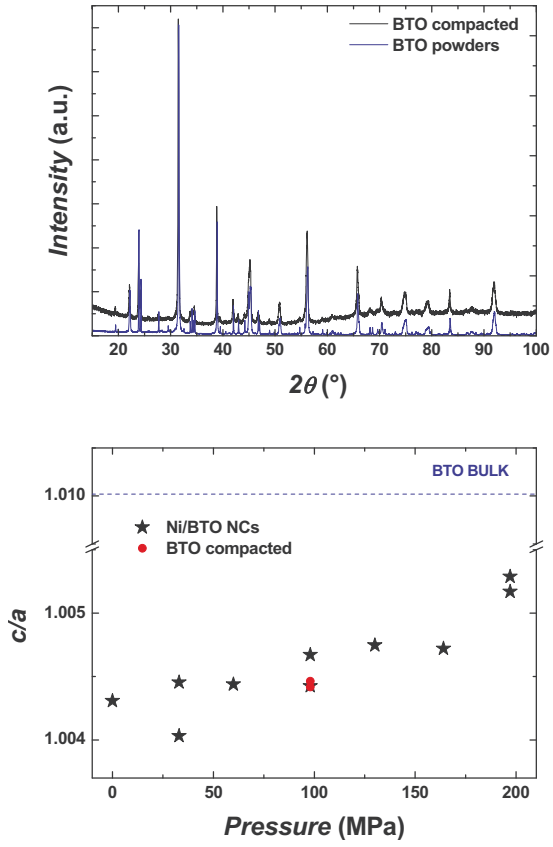

FIG. 3. (Color online) Upper panel: x-ray diffraction patterns of the $BaTiO_3$ powder (lower trace) and $BaTiO_3$ compact (upper trace) as a function of the x-ray 2θ diffraction angle. The labels identify various peaks in the spectra. Room temperature under air ambient. Lower panel: evolution of the measured tetragonality ratio c/a calculated from the (200) and (002) Bragg peaks for the $BaTiO_3$ phase in the $Ni/BaTiO_3$ NC containing 17.1 vol % of Ni at room temperature as a function of the pressure applied during powder compaction (98 MPa). The dashed line corresponds to the bulk value of c/a for $BaTiO_3$.

PROF suite package by employing the full-profile Rietveld refinement. As an illustrative example, the room temperature XRD patterns of the $BaTiO_3$ powder and compact are displayed in Fig. 3(a) and show weak contaminant peaks characteristic of the $BaCO_3$ compound. Ni particles are polycrystalline and there is no preferred orientation in the samples. For Ni, there were no peaks in the diffraction data (not shown) that could not be assigned to magnetic impurities. The average particle sizes were calculated using the full width at half maximum (FWHM) using the Scherrer equation. These calculations, i.e., 39 nm and 25 nm for $BaTiO_3$ and Ni, respectively, are consistent with the data taken using the microscopy measurements and the manufacturer product literature. In this figure, all diffraction peaks were indexed to the tetragonal structure, in agreement with the respective joint committee on powder diffraction standards.[33] For the $BaTiO_3$ phase, no significant p dependence (not shown) was found on $a=4.003\pm0.002$ Å. There is no degradation of the primary phases due to the fabrication process. Figure 3(b) shows the tetragonality ratio c/a as function of p. Upon increasing p the slight tetragonal distortions of the unit-cell results in a small increase in c/a. However, in the pressure range explored, this value remains smaller than the corresponding bulk value. A comparison of the DRX pattern for compacted powder of $BaTiO_3$ is shown in Fig. 3(a).

The samples were examined by microwave spectroscopy, and magnetization techniques. The experimental setup used to observe GHz ε and μ has been described in detail elsewhere.[2–5,34] Briefly, a transmission/reflection method has been employed. This experimental technique is based on the measurement of the scattering parameters of a toroidal sample of the test material which has been machined in order that the geometrical dimensions fit well those of the coaxial line used (to avoid the presence of air gaps between the sample and the line walls). In this coaxial air-line measurement the fundamental transverse electromagnetic TEM mode is the only mode that propagates in the coaxial line. An error analysis indicates systematic uncertainties in ε' (<5%), ε'' (<1%), μ' (<3%), and μ'' (<1%) for the data. A Agilent 8753 ES network analyzer setup is used to measure the S parameters of the cell containing the material under test over a wide range of frequencies (100 MHz–6 GHz). We apply the short-open-load-though calibration to the measurement since this method permits error correction over a wide frequency band. The size of the particles is below skin depth up to optical frequencies. The magnetic properties (M-H loops) were measured at room temperature by standard VSM using parallelepipedic samples with nominal dimensions $1\times4\times3$ mm^3. All the measurements were performed by applying the magnetic field in the plane of the sample [with reference to the schematic representation of the experimental measurement given in Fig. 4(a)]. The information on magnetic anisotropy can be obtained directly by studying the dependence of the magnetization on the direction of the applied magnetic field. Hysteresis loops were measured with a maximum magnetic field of 6 kOe at room temperature.

III. RESULTS AND DISCUSSION

A. Orientation and pressure dependence of static magnetization properties

Previous works on ME NCs have emphasized static magnetization properties.[2–6,14,15,35] The magnetic data shown in Ref. 5, for $p=98$ MPa, indicates that they can be understood by an overall dilution of the magnetic phase. However, the results of the VSM magnetization measurements observed here cannot be totally explained by the demagnetization process of noninteracting Ni particles. Therefore, this result suggests that some interaction exists between the Ni boundary structures (aggregates). Various parameters derived from the magnetic hysteresis curves are shown in Figs. 4–6. We begin describing the results with data showing that the compaction pressure affects significantly the isothermal magnetization data. The remarkable feature of Fig. 4(b) is the observation of a small decrease in the coercivity upon increasing p. In addition it remains almost constant over the range of θ explored. One can see in Fig. 4(c) that the squareness is significantly much smaller than the value predicted by the Wolfarth model predicting $M_r/M_s=0.5$ for a random distribution of noninteracting uniaxial single domain particles, with coherent rotation of the magnetization. We believe that this deviation from this ideal value is due to interparticle

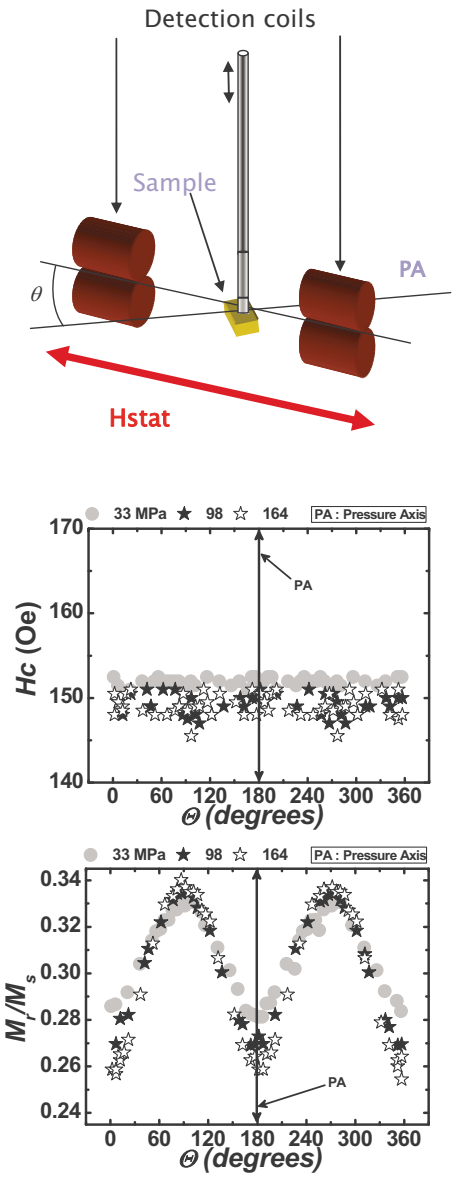

FIG. 4. (Color online) Upper panel: schematic description of the experimental setup, consisting of an electromagnet, and a sample holder used to record the M-H loops. It shows how the polar angle θ is defined. PA means compaction pressure axis. Middle panel: coercivity (H_c) as a function of the angle θ for the $BaTiO_3$/Ni NC sample containing 17.1 vol % of Ni and selected values of the compaction pressure. The numbers in the graph indicate the compaction pressure. Room temperature. Lower panel: same as in (a) for the squareness (M_r/M_s).

interactions as a consequence of aggregation within the host matrix. Figure 5(a) shows pressure-dependent squareness data for two values of angle indicating the presence of a strong interfacial-like anisotropy. M_r/M_s has a form of a figure-of-eight when viewed on a polar plot [Fig. 5(b)]. This graph illustrates how much the change in the anisotropy of the magnetic component is because it is strained during compaction. Further insight can also be gained from Fig. 6. As expected, the addition of Ni produces a decrease in the coercive field [Fig. 6(a)] and no angular dependence can be observed. The reduced squareness observed in Fig. 6(b) might result from the polycrystalline and interface-related structural imperfections.

As is well documented in the literature, the stress state in a magnetic structure can have a pronounced effect on the

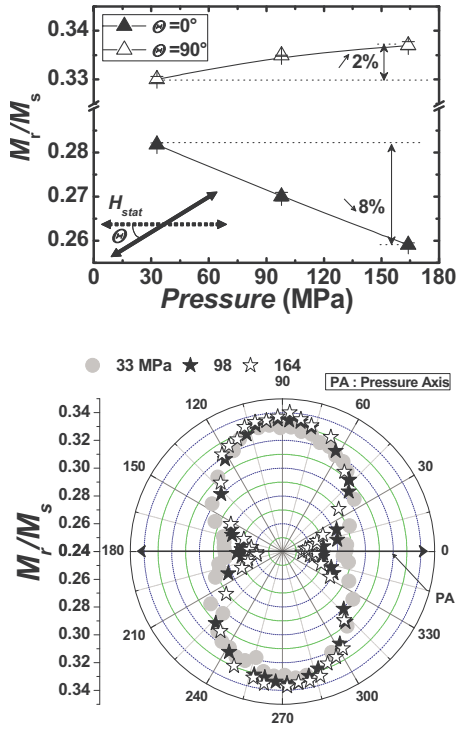

FIG. 5. (Color online) Upper panel: squareness as a function of the compaction pressure for two values of θ for the $BaTiO_3$/Ni NC sample containing 17.1 vol % of Ni. PA means compaction pressure axis. Lower panel: polar plot illustrating the distribution of M_r/M_s.

magnetic properties, and hence on the several contributions to its magnetic anisotropy, i.e., strain anisotropy, magnetocrystalline anisotropy.[36] It is worth noting that the residual stresses are related to extrinsic stress, i.e., difference between thermal expansion coefficient of the two phases in the NCs, and intrinsic stress, e.g., stress related to defect incorporation, phase transition stress due to orientation change. The

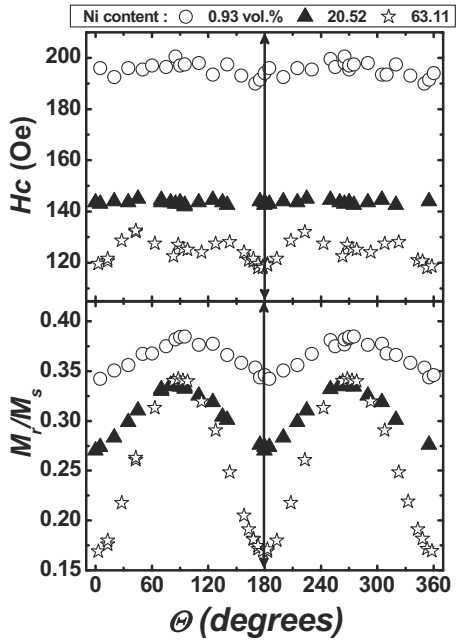

FIG. 6. Upper panel: coercivity vs θ at different Ni contents. The compaction pressure used during the fabrication of the samples is 98 MPa. Lower panel: squareness vs θ at different Ni contents.

observed magnetic anisotropy is unlikely due to the small variation in the crystallographic parameters under compression as shown in Fig. 3(b). Compaction will induce a stress in the magnetic material and this stress will be relieved by strains in both components of the composite. In summary, it appears plausible that the grain orientation change during compressive stress will affect local anisotropy distributions, and consequently the effective magnetization properties of the NCs.

B. Room temperature ME properties

The ME behavior in multiphase composites is strongly dependent on their microstructure and coupling interaction across the piezoelectric/magnetostrictive interface, it is expected that residual stress generated during the fabrication process can be responsible for the eventual nucleation, evolution, and coalescence of voids. These factors strongly hinder the domain reorientation, and therefore limiting the polarization process.

We now turn to a discussion of the complex effective (relative) permittivity with a systematic variation in compaction pressure of the APC-7-sized samples. Figure 7 shows a comparison of the resonance characteristics, i.e., the imaginary part of the effective permittivity at resonance, $\varepsilon_r''=\varepsilon_r''(F_r)$, the ME coefficient, $\alpha_\varepsilon''=(\partial\varepsilon_r''/\partial H)_T$, the resonant frequency F_r, and the FWHM, ΔF, as a function of the dc magnetic field at a fixed composition (17.1 vol % of Ni in the $BaTiO_3$/Ni NC sample) and several nominal values of p. We observe experimentally that the main feature common to the plots in Fig. 7 is that a change of a factor of 6 of pressure has a significant effect on the resonance frequency peak position and the coupling coefficients. Similar results were obtained for a range of different Ni loading. Overall, one can say that the most interesting result observed is that the maximum α_ε'' value at resonance, is found for a specific pressure ($\approx$98 MPa) above which the ME coupling does not increase. This ME coefficient is large and is comparable to recently reported measurements in $BiFeO_3/CoFe_2O_4$ NCs.[17]

Lastly, we give an illustration in Fig. 8 of how α_ε'', F_r, and ΔF vary with compaction pressure. A perusal of the data of the upper panel of Fig. 8 shows that the appropriate compaction pressure can improve significantly the value of α_ε''. Remarkably, the redshift of F_r as p varies by a factor of 6 indicates is likely due to the large porosity, intergranular stress associated with the grain boundary, and impurities, which result from the embedding process.[37,38] These factors strongly hinder the domain reorientation, and give rise to both local demagnetization and depolarization. In the lower panel of Fig. 8, we also observe that not only ΔF is almost constant versus p, but the value of ΔF is found very close to that corresponding to neat $BaTiO_3$ if the applied magnetic field is larger than 3 kOe.

C. Further discussion

Coming to an overall discussion of our results, one should keep in mind that the functionalities of the Ni nanoparticles are strongly correlated with their local collective magnetic behavior. We have already alluded to the fact that

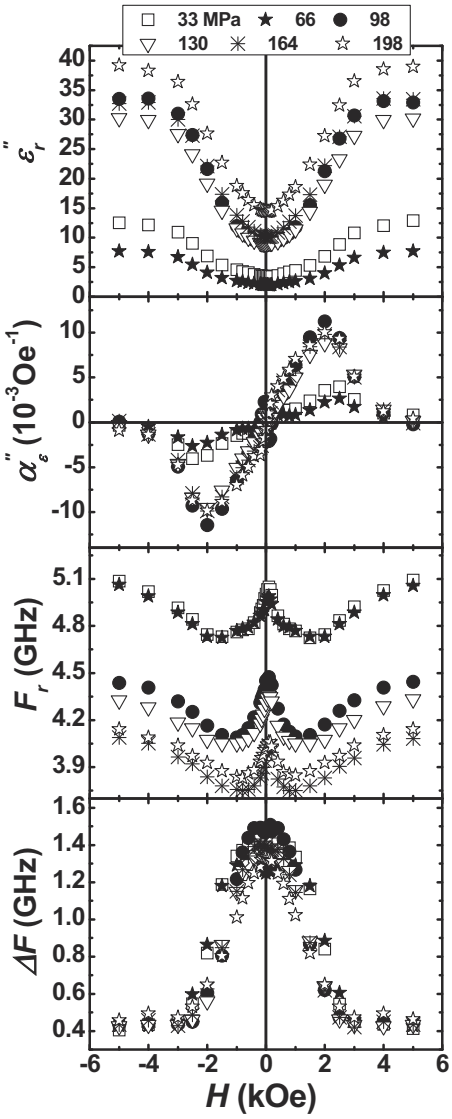

FIG. 7. (a) The effective permittivity, $\varepsilon_r''=\varepsilon_r''(F_r)$, at the resonance frequency as a function of the dc magnetic field for $BaTiO_3$/Ni NC sample containing 17.1 vol % of Ni. The numbers in the graph indicate the compaction pressure. Room temperature. (b) $\alpha_\varepsilon''=(\partial\varepsilon_r''/\partial H)_T$ as a function of the dc magnetic field. (c) The resonant frequency F_r as a function of the dc magnetic field. (d) The FWHM, ΔF, as a function of the dc magnetic field.

the extrinsic ME effect can be attributed to the interplay between the dipole interactions and lattice strain. In these complex composite materials minority phase formed by Ni nanoclusters induce local strain due to their lattice mismatch with the $BaTiO_3$ host matrix that tend to break the dipole pairing pattern. Likewise, magnetic anisotropies in nanostructures can be associated with the structure stresses and morphology of the materials. While it is known that scanning probe techniques such as SEM and magnetic force microscopy (MFM) are generally difficult to be used for structural characterization of nanostructures due to the significant interference of the morphological corrugation, roughness is expected to increase inhomogeneity of the magnetic properties. In addition, when attempting to understand the properties of polycrystalline materials, one is faced with the problem that real materials usually contain a variety of different boundary structures. Various factors, including the presence of impuri-

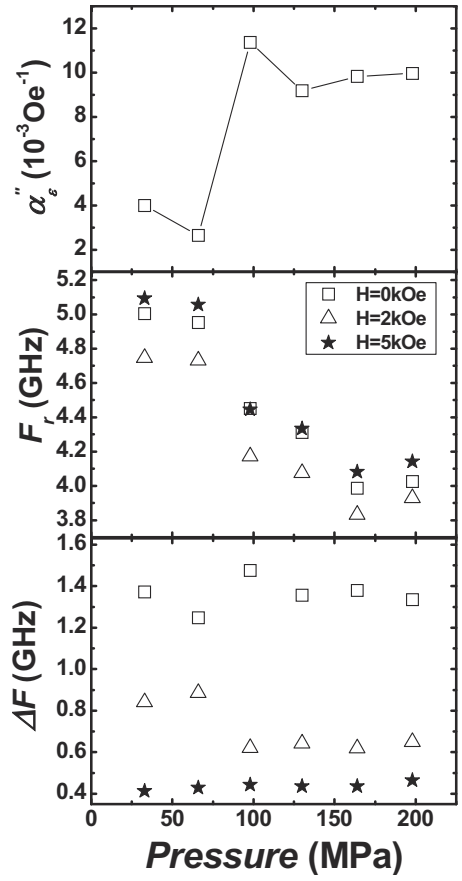

FIG. 8. Upper panel: $\alpha''_\varepsilon=(\partial\varepsilon''_r/\partial H)_T$ for the $BaTiO_3$/Ni NC sample containing 17.1 vol % of Ni as a function of the compaction pressure. The numbers in the graph indicate the applied magnetic field. Room temperature. Middle panel: the resonant frequency F_r as a function of the dc magnetic field. Lower panel: the FWHM, ΔF, as a function of the dc magnetic field.

ties, compaction pressure, influence both the types of boundary present and their relative concentrations. Defects and impurities in polycrystalline materials favorably segregate grain boundaries and decreased density at the boundary. The random grain orientation may affect magnetic properties in ME NCs through various processes: the grain orientation directly affects the anisotropy of individual nanoparticles via interfacial and/or magnetocrystalline anisotropy effects. It was recognized that the ME effect may originate from purely electronic mechanisms at ferromagnet/insulator interfaces. Hence, displacements of atoms at the ferromagnetic/ferroelectric interface alter the overlap between atomic orbitals at the interface which affects interface magnetization.[39] The ME effect due to interface bonding mechanism is expected to play a role for $Fe/BaTiO_3$, and $Fe_3O_4/BaTiO_3$ interfaces.[39]

As the next item for discussion, we have shown in Sec. III B that the effective permittivity at microwave frequencies can be controlled by an external magnetic field. Possible mechanisms which can induce the ME effect are magnetoresistance, magnetocapacitance, or indirect coupling between magnetization and polarization through elastic strain.[7] The absence of magnetic field dependence of the electrical-resistivity between zero and ± 10 kOe rules out magnetoresistance as the origin of the ME effect.[5] We also excluded magnetocapacitance as a source of the ME effect because $[\varepsilon(H)-\varepsilon(0)]/\varepsilon(0)$ does not evidence quadratic magnetization dependence as pointed out by several previous studies.[40] We showed that one likely scenario that can explain our results is to consider that the applied magnetic field induces strain in the magnetostrictive constituent which is mechanically transferred to the piezoelectric constituent where it induces a polarization. The strain caused by a magnetic field in these materials is not linearly proportional to the field strength but is related to the square of the magnetic field strength.[41,42] We mention parenthetically that most real multiferroic materials have either small ε or μ and their linear (direct) ME coupling is usually weak.

Before finishing this section, an important remark regarding our choice to focus on the NC containing 17.1 vol % of Ni should be made. In a recent study,[5] we showed that the dc conduction transition observed in the $Ni/BaTiO_3$ NC containing 17.1 vol % of Ni leads to a change of conductivity by four orders of magnitude and is believed to be associated with an insulator-conductor transition. This specific Ni content corresponds to the peak in the magnitude of the ME coefficient at room temperature (Fig. 16 of Ref. 5). Still regarding the interface effect in the microscopic origin of the ME coupling, we also point out that at percolation threshold there is an infinite cluster of connected aggregates which is characterized by a fractal geometry known to maximize the surface area to volume ratio of these structures.

IV. SUMMARY

In summary, a combination of several complementary experimental techniques has been used to investigate a series of $BaTiO_3/Ni$ NCs produced by compaction of nanopowders. The different probes have been used to ascertain that the striction across the interfaces between the magnetic and piezoelectric phases is the relevant physical mechanism that underlies the ME effect in these materials. The main message to emerge from this work is that the microwave properties of NCs can be greatly modified by the compaction pressure used during production of the NCs. Under compressive stress Ni grain boundaries induce significant variations in the magnetic anisotropy which is assumed to reside solely in the Ni nanoparticles and aggregates and interfaces. The magnetization properties are determined by the interplay of several anisotropies among which strain anisotropy plays a significant role. Local inhomogeneities in the strain due to crystalline defects or grain boundaries can produce local fluctuations in the magnetic anisotropy direction. If the average magnetization is the result of local moments present at defects, then it is essential to establish which defects actually occur and to determine the mechanism underpinning their long-range magnetic coupling. These magnetically stressed and compacted NCs exhibit a large enhancement of the ME coupling coefficient $\alpha_\varepsilon=(\partial\varepsilon/\partial H)_T$. It is demonstrated that appropriate compaction pressure can improve the value of α_ε. To reiterate, these observations and the local nature of the interfacial anisotropy can be rationalized on the basis of the stress-induced microstructural changes under pressure which strongly affect the elastic interactions between the magneto-

strictive and piezoelectric phases in these nanostructures. Grain boundaries in these systems can be both beneficial and harmful to ME applications. The next challenging task is to establish a connection between the features obtained here and the electric field-induced ME effect, i.e., ferroelectric polarization.

Before ending, we note that the results reported here are anticipated to support future research in at least three aspects. (1) So for ME NCs technological applications to progress further over the coming years, a better understanding of the factors that affect electric polarization, e.g., magnetic effects on the *P-E* hysteresis loops, needs to be determined. The full body of data presented here constitutes a basis to investigate the physical properties of other ME NCs. (2) Advances in techniques for controllable epitaxial strain in laminate nanostructures[43–45] with alternating layers of $BaTiO_3$ and Ni make the comparison with these NCs particularly challenging. Clearly this will provide a different configuration of surface interface regions, giving all possible angular variations with respect to the magnetization. (3) Finally, with constantly increasing demand for "smarter" composites, these materials provide a potential usage as building blocks for specific multifunctional materials and can be exploited in a number of microwave and millimeter wave devices such as tunable phase shifters, resonators, and delay lines. There has been a limited attempt to use the capabilities of these NCs for cost effective, small size, and broadband devices. Nevertheless, there is a fast growing literature in this area that will eventually tell us much more about the usefulness of these amazing materials. A more careful treatment of the insertion loss, and planar integrability in devices using these materials will be left for further investigation.

ACKNOWLEDGMENTS

This work was made possible by support through a Conseil Régional de Bretagne grant to V. C. We would like to thank J. Ben Youssef for technical assistance in acquiring the VSM data. We have benefited of technical support from G. Sinquin and P. Elies. Lab-STICC is UMR CNRS 3192. Unité Sciences Chimiques de Rennes is UMR CNRS 6226.

[1]C.-W. Nan, M. I. Bichurin, S. Dong, D. Viehland, and G. Srinivasan, J. Appl. Phys. **103**, 031101 (2008).
[2]V. Castel, J. Ben Youssef, and C. Brosseau, J. Nanomater. **2007**, 16 (2007), article ID 27437.
[3]V. Castel and C. Brosseau, Phys. Rev. B **77**, 134424 (2008).
[4]V. Castel and C. Brosseau, Appl. Phys. Lett. **92**, 233110 (2008).
[5]V. Castel, C. Brosseau, and J. Ben Youssef, J. Appl. Phys. **106**, 064312 (2009).
[6]J. Das, B. A. Kalinikos, A. R. Barman, and C. E. Patton, Appl. Phys. Lett. **91**, 172516 (2007).
[7]W. Eerenstein, N. D. Mathur, and J. F. Scott, Nature (London) **442**, 759 (2006); J. F. Scott, Nature Mater. **6**, 256 (2007); J. F. Scott, Science **315**, 954 (2007); M. Dawber, K. M. Rabe, and J. F. Scott, Rev. Mod. Phys. **77**, 1083 (2005); N. A. Hill, J. Phys. Chem. B **104**, 6694 (2000).
[8]J. Helszajn, *YIG Resonators and Filters* (Wiley, New York, 1985).
[9]M. I. Bichurin, V. M. Petrov, Y. V. Kiliba, and G. Srinivasan, Phys. Rev. B **66**, 134404 (2002).
[10]M. Fiebig, J. Phys. D **38**, R123 (2005).
[11]S. W. Cheong and M. Mostovoy, Nature Mater. **6**, 13 (2007).
[12]C. Brosseau and P. Talbot, IEEE Trans. Dielectr. Electr. Insul. **11**, 819 (2004); P. Talbot, A.-M. Konn, and C. Brosseau, J. Magn. Magn. Mater. **249**, 481 (2002).
[13]C. Brosseau and P. Talbot, J. Appl. Phys. **97**, 104325 (2005).
[14]C. Brosseau, J. Ben Youssef, P. Talbot, and A.-M. Konn, J. Appl. Phys. **93**, 9243 (2003).
[15]J. Ben Youssef and C. Brosseau, Phys. Rev. B **74**, 214413 (2006).
[16]H. Zheng, J. Wang, L. Mohaddes-Ardabili, M. Wuttig, L. Salamanca-Riba, D. G. Schlom, and R. Ramesh, Appl. Phys. Lett. **85**, 2035 (2004).
[17]F. Zavaliche, H. Zheng, L. Mohaddes-Ardabili, S. Y. Yang, Q. Zhan, P. Shafer, E. Reilly, R. Chopdekar, Y. Jia, D. G. Schlom, Y. Suzuki, and R. Ramesh, Nano Lett. **5**, 1793 (2005).
[18]H. Zheng, F. Straub, Q. Zhan, P.-L. Yang, W.-K. Hsieh, F. Zavaliche, Y.-H. Chu, U. Dahmen, and R. Ramesh, Nano Lett. **6**, 1401 (2006).
[19]H. M. Luo, H. Yang, S. C. Baily, O. Ugurlu, M. Jain, M. E. Hawley, T. M. McCleskey, E. Bauer, L. Civale, T. G. Holesinger, and Q. X. Jia, J. Am. Chem. Soc. **129**, 14132 (2007).
[20]I. Levin, J. H. Li, J. Slutsker, and A. L. Roytburd, Adv. Mater. (Weinheim, Ger.) **18**, 2044 (2006).
[21]H. Zheng, J. Wang, S. E. Lofland, Z. Ma, L. M. Ardabili, T. Zhao, L. Salamanca-Riba, S. R. Shinde, S. B. Ogale, F. Bai, D. Viehland, Y. Jia, D. G. Schlom, M. Wuttig, A. Roytburd, and R. Ramesh, Science **303**, 661 (2004).
[22]R. A. Islam, D. Viehland, and S. Priya, J. Mater. Sci. **43**, 1497 (2008).
[23]R. A. Islam, Y. Ni, A. G. Khachaturyan, and S. Priya, J. Appl. Phys. **104**, 044103 (2008).
[24]Y. Chen, X.-Y. Zhang, C. Vittoria, and V. G. Harris, Appl. Phys. Lett. **94**, 102906 (2009).
[25]L. C. Chapon, G. R. Blake, M. J. Guttman, S. Park, N. Hur, P. G. Radaelli, and S. W. Cheong, Phys. Rev. Lett. **93**, 177402 (2004).
[26]C. dela Cruz, F. Yen, B. Lorenz, Y. Q. Wang, Y. Y. Sun, M. M. Gospodinov, and C. W. Chu, Phys. Rev. B **71**, 060407(R) (2005); C. dela Cruz, F. Yen, B. Lorenz, M. M. Gospodinov, C. W. Chu, W. Ratcliff, J. W. Lynn, S. Park, and S. W. Cheong, *ibid.* **73**, 100406(R) (2006).
[27]S. Lee, A. Pirogov, M. Kang, K.-H. Jang, M. Yonemura, T. Kamiyama, S. W. Cheong, F. Gozzo, N. Shin, H. Kimura, Y. Noda, and J.-G. Park, Nature (London) **451**, 805 (2008).
[28]E. Montanari, G. Calestani, L. Righi, E. Gilioli, F. Bolzoni, K. S. Knight, and P. G. Radaelli, Phys. Rev. B **75**, 220101(R) (2007).
[29]E. Dagotto, Science **318**, 1076 (2007).
[30]L. Lutsev, S. Yakovlev, V. Castel, and C. Brosseau (unpublished).
[31]N. P. Young, Z. Y. Li, Y. Chen, S. Palomba, M. Di Vece, and R. E. Palmer, Phys. Rev. Lett. **101**, 246103 (2008).
[32]*Granular Matter: An Interdisciplinary Approach*, edited by A. Mehta (Springer-Verlag, New York, 1994); A. Malliaris and D. T. Turner, J. Appl. Phys. **42**, 614 (1971).
[33]Joint Committee on Powder Diffraction Standards, International Centre for Diffraction Data (Newton Square, PA, 2001).
[34]R. E. Collin, *Foundations for Microwave Engineering*, 2nd ed. (Wiley, New Jersey, 2000); D. M. Pozar, *Microwave Engineering*, 3rd ed. (Wiley, New Jersey, 2005).
[35]B. D. Cullity, *Introduction to Magnetic Materials* (Addison-Wesley, Reading, MA, 1972).
[36]S. S. Kalarickal, D. Ménard, J. Das, C. E. Patton, X. Zhang, L. C. Sengupta, and S. Sengupta, J. Appl. Phys. **100**, 084905 (2006).
[37]J. Baker-Jarvis and P. Kabos, Phys. Rev. E **64**, 056127 (2001).
[38]S. Wan and K. J. Bowman, J. Mater. Res. **16**, 2306 (2001); K. Uchino, E. Sadanaga, and T. Hirose, J. Am. Ceram. Soc. **72**, 1555 (1989).
[39]C.-G. Duan, S. S. Jaswal, and E. Y. Tsymbal, Phys. Rev. Lett. **97**, 047201 (2006); M. Fechner, I. V. Maznichenko, S. Ostanin, A. Ernst, J. Henk, P. Bruno, and I. Mertig, Phys. Rev. B **78**, 212406 (2008); M. K. Niranjan, J. P. Velev, C.-G. Duan, S. S. Jaswal, and E. Y. Tsymbal, *ibid.* **78**, 104405 (2008).
[40]G. Catalan, Appl. Phys. Lett. **88**, 102902 (2006); V. Laukhin, B. Martinez, J. Fontcuberta, and Y. M. Mukovskii, Phys. Rev. B **63**, 214417 (2001).
[41]J.-W. G. Bos, C. V. Colin, and T. T. M. Palstra, Phys. Rev. B **78**, 094416 (2008).
[42]D. Stauffer and A. Aharony, *Introduction to Percolation Theory* (Taylor & Francis, London, 1994).
[43]W. Tian, V. Vaithyanathan, D. G. Schlom, Q. Zhan, S. Y. Yang, Y. H. Chu, and R. Ramesh, Appl. Phys. Lett. **90**, 172908 (2007).
[44]J. Wang, J. B. Neaton, H. Zheng, V. Nagarajan, S. B. Ogale, B. Liu, D. Viehland, V. Vaithyanathan, D. G. Schlom, U. V. Waghmare, N. A. Spaldin, K. M. Rabe, and R. Ramesh, Science **299**, 1719 (2003).
[45]R. Wiesendanger, *Scanning Probe Microscopy and Spectroscopy: Methods and Applications* (Cambridge University Press, Cambridge, 1994).